

UC Santa Barbara

UC Santa Barbara Previously Published Works

Title

Solid Electrolytes in the Spotlight

Permalink

<https://escholarship.org/uc/item/888980w2>

Journal

Chemistry of Materials, 34(2)

ISSN

0897-4756

Authors

Doeff, Marca M
Clément, Raphaële J
Canepa, Pieremanuele

Publication Date

2022-01-25

DOI

10.1021/acs.chemmater.1c03770

Peer reviewed

This document is confidential and is proprietary to the American Chemical Society and its authors. Do not copy or disclose without written permission. If you have received this item in error, notify the sender and delete all copies.

Solid Electrolytes in the Spotlight

Journal:	<i>Chemistry of Materials</i>
Manuscript ID	cm-2021-03770u
Manuscript Type:	Editorial
Date Submitted by the Author:	31-Oct-2021
Complete List of Authors:	Doeff, Marca; E O Lawrence Berkeley National Laboratory, Energy Storage and Distributed Resources Division Clément, Raphaële; University of California Santa Barbara, Materials Canepa, Pieremanuele; National University of Singapore, Materials Science and Engineering

SCHOLARONE™
Manuscripts

Solid Electrolytes in the Spotlight

Marca M. Doeff,^{*,†} Raphaële J. Clément,^{*,‡,§} and Pieremanuele Canepa^{*,¶,||}

[†]*Lawrence Berkeley National Laboratory, Energy Storage and Distributed Resources Division, Berkeley, CA 94720, USA*

[‡]*Materials Department, University of California, Santa Barbara, CA 93106, USA*

[¶]*Department of Materials Science and Engineering, National University of Singapore, 9 Engineering Drive 1, 117575, Singapore*

[§]*Materials Research Laboratory, University of California, Santa Barbara, CA 93106, USA*

^{||}*Department of Chemical and Biomolecular Engineering, National University of Singapore, 4 Engineering Drive 4, 117585, Singapore*

E-mail: mmdoeff@lbl.gov; rclement@ucsb.edu; pcanepa@nus.edu.sg

This virtual issue is targeted to students and researchers, and highlights 31 research articles published over the past 5 years (from July 2016 to July 2021) in Chemistry of Materials (CM). The compilation of papers summarizes the latest advances in the field of solid-state electrolytes for lithium (Li)-, sodium (Na)- and multivalent-ion (not among the 31 articles discussed) all-solid-state batteries (ASSBs), with a focus on inorganic materials and excluding hybrid systems, e.g., polymer/ceramic composites or systems including liquid media. A total of 125 articles reporting exciting experimental and/or theoretical findings on solid electrolytes have been considered for this issue. During 2017-2019, there were about 25-30 papers published per year on this topic, but 2020 and 2021 saw a significant increase, with 26 publications in the first half of 2021 alone. Submissions came from many countries around the globe, as shown in Figure 1. While most papers were led by research groups located in the United States, Germany and Japan follow closely, and Austria, the United Kingdom, Canada, and China are also well represented.

By far the largest number of CM articles concern solid-state electrolytes for Li-ion battery applications (94 papers), with Na-ion conductors (25 papers) a distant second. Electrolytes for multivalent systems (Mg^{2+} , Ca^{2+} and Zn^{2+})

and fluoride ion conductors remain niche topics (6 papers).

Sulfide-based solid electrolytes have been under intense scrutiny as many demonstrate remarkably high ionic conductivities at room temperature (some even higher than that of common liquid electrolytic solutions) and can be prepared in dense pellets without the need for sintering. Nonetheless, most sulfide electrolytes are unstable in air and/or suffer from poor anodic and cathodic stabilities, which may hinder their practical application. While 54 papers have been published on Li-ion conducting sulfides, Na-based sulfides and their applications in Na ASSBs have also received significant attention.^{1? -5} Through a multi-technique approach, including Raman spectroscopy, pair-distribution function analysis, inelastic neutron scattering, and density functional theory (DFT), X-ray diffractions (XRD), differential scanning calorimetry, Famprakis and collaborators⁴ have disentangled the much debated crystal symmetry of the high-conductivity “cubic”- Na_3PS_4 phases and the second-order phase-transition tetragonal-to-cubic, which is responsible for the material outstanding ionic conductivities ($\sim 10^{-4}$ S/cm). Raman spectroscopy was crucial to observing that the “cubic”- Na_3PS_4 phases contains remnants of tetragonal character,⁴ which aids Na-ion transport at

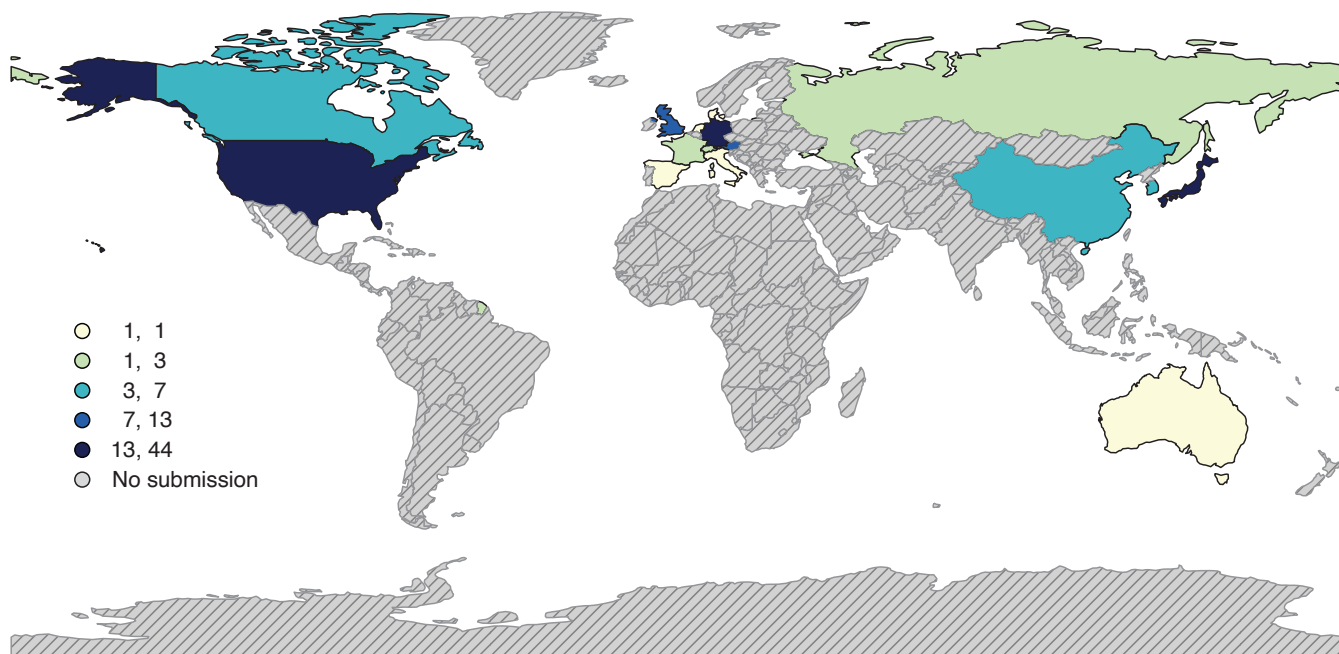


Figure 1: Global distribution of research activities on all solid-state electrolytes published in CM over the past 5 years. Grey hatched areas show countries without publications on this topic in CM.

higher temperatures. This study emphasizes that the usual combination of powder XRD and electrochemical impedance spectroscopy (EIS) alone is not sufficient to reveal the complex interplay of structure and ionic conductivity in solid electrolytes. Other chalcogenide solid electrolytes, $\text{Na}_{11}\text{Sn}_2\text{XS}_{12}$ or $\text{Na}_{11}\text{Sn}_2\text{XSe}_{12}$ (with $\text{X}=\text{P}$ and Sb), have demonstrated impressive Na-ion conductivities ($1\text{--}4\text{ mS/cm}$),^{5,7} but are unstable in the presence of oxygen and moisture. Based on the idea that “soft acid” sulfides are more stable under ambient conditions, Ramos et al.⁵ developed an antimony-based $\text{Na}_{11}\text{Sn}_2\text{SbS}_{12}$ analog, with good structural stability and a marginal decrease in Na-ion conductivity after being exposed to dry air for 36 hours.

Among the novel and rediscovered solid electrolyte chemistries, oxy/hydroxyhalides and halides have shown particular promise. Oxy/hydroxyhalides with the anti-perovskite structure offer high ionic conductivities on the order of mS/cm . Li-rich anti-perovskites (e.g., $\text{Li}_{3-x}(\text{OH}_x)\text{Cl}$) are of interest due to their low cost, but their synthesis requires stringent conditions and their exact composition, structure, and ion conduction mechanism re-

main unclear. Hanghofer et al.⁶ have examined a range of Li-OH-Cl anti-perovskites using neutron diffraction and NMR. They reported the first structural models for the cubic and a new orthorhombic phases, which also contained structural information about the H atoms in the framework. Their work indicates that $\text{Li}_4(\text{OH})_3\text{Cl}$ and variants of $\text{Li}_{3-x}(\text{OH}_x)\text{Cl}$ where $x > 0$ are the only stable Li-rich anti-perovskites.⁶ Using complementary experimental and computational methods, Wang and collaborators have shown that the high Li-ion conductivity in Li_2OHCl is correlated to the “paddlewheel” rotation of the OH^- anions.⁷

Rocksalt-type lithium ternary halide electrolytes (with general formula Li_3MX_6) have also attracted significant attention over the past few years. A computational study of the phase and electrochemical stability by Yu and coworkers has predicted that chlorides have the highest oxidation potential ($\sim 4.3\text{ V}$ vs. Li/Li^+) and elastic moduli within this class of materials, making them particularly compatible with high-voltage cathodes.⁸ Additionally, aliovalent substitution of M^{3+} for Zr^{4+} is expected to enhance Li-ion conduction, resulting in low diffusion barriers ($\sim 0.25\text{ eV}$). These predictions have

1 been confirmed by Helm et al.,⁹ who explored
2 the series of $\text{Li}_{3-x}\text{In}_{1-x}\text{Zr}_x\text{Cl}_6$ electrolytes and
3 demonstrated, using high-resolution diffraction
4 data, the presence of a new tetrahedrally-
5 coordinated Li position together with cation
6 disorder. These structural features together
7 with the increase in the number of vacancies
8 led to the formation of a 3D Li-ion diffusion
9 network and increased room temperature Li-ion
10 conductivity.

11 The development of design rules for solid elec-
12 trolytes hinges on an understanding of the elec-
13 trolyte composition, structure, and microstruc-
14 ture and how these affect the conduction of
15 ions, the mechanical properties and the thermal
16 and electrochemical stabilities towards elec-
17 trode materials. Besides diffraction techniques,
18 solid-state NMR (SS-NMR) has emerged as an
19 important tool to investigate the local struc-
20 ture of solid electrolytes and provides quantita-
21 tive information on both crystalline and amor-
22 phous phases present in the sample. Using SS-
23 NMR, Harm et al. identified a low conductiv-
24 ity amorphous thiophosphate phase with low Si
25 content in tetragonal Li_7SiPS_8 ,¹⁰ a new member
26 of the $\text{Li}_{10}\text{GeP}_2\text{S}_{12}$ (LGPS)-type family. This
27 impurity resulted in limited inter-granular con-
28 ductivity, explaining the unexpectedly low bulk
29 conductivity observed with impedance spec-
30 troscopy. This case study highlights the need
31 for comprehensive structural analysis of glass-
32 ceramic compounds beyond the crystalline frac-
33 tions.¹⁰ SS-NMR is also an indispensable tool
34 for the characterization of chalcogenide glasses,
35 as exemplified by Marple and coworkers for
36 the study of the $\text{Li}_2\text{S}-\text{Ga}_2\text{Se}_3-\text{GeSe}_2$ family of
37 compounds.¹¹

38 The study by Wang et al.⁷ emphasized the
39 role of anion rotations in the mechanism of Li-
40 ion conduction in the anti-perovskite Li_2OHCl
41 electrolyte. Variable-temperature X-ray and
42 neutron diffraction experiments, and EIS were
43 essential for correlating an orthorhombic to cu-
44 bic phase transition with an ~ 100 -fold increase
45 in ionic conductivity near 311 K. Furthermore,
46 quasi-elastic neutron scattering, maximum en-
47 tropy method analysis of the neutron diffraction
48 data, and *ab initio* molecular dynamics simu-
49 lations (AIMD) together correlated fast Li-ion
50

diffusion with the local rotations of framework
51 OH^- anions. This work illustrates the power
52 of combining experimental and computational
53 tools to probe dynamic processes over a range
54 of length and timescales. By far the most com-
55 monly used tool for probing bulk ionic con-
56 ductivity is EIS; here, we recommend a Meth-
57 ods/Protocols article by Krasnikova et al.¹²
58 that proposes a unified approach towards ob-
59 taining reliable EIS data on ion-conducting ce-
60 ramics, verifying the equivalent circuit by ad-
61 justing the temperature, and estimating errors
62 in measurements.

The identification of electrolyte degradation
63 pathways during handling and processing is key
64 to the development of effective manufacturing
65 protocols. Using a combination of *operando*
66 optical microscopy, Raman spectroscopy, syn-
67 chrotron XRD, and in situ XANES, Sun and
68 coworkers showed that rocksalt-type Li_3InCl_6
69 reacts with water upon air exposure, which re-
70 duces drastically its ionic conductivity.¹³ While
71 In_2O_3 , LiCl and HCl formed at the surface of
72 the particles upon reaction with adsorbed wa-
73 ter, H_2O molecules inserted into the particles
74 and led to $\text{Li}_3\text{InCl}_6 \cdot x\text{H}_2\text{O}$ hydrates. Likewise,
75 Sharafi et al.¹⁴ and Brugge et al.¹⁵ using XPS
76 have demonstrated that $\text{Li}_7\text{La}_3\text{Zr}_2\text{O}_{12}$ (LLZO)
77 reacts vigorously with CO_2 and H_2O at ambi-
78 ent conditions, with significant effects on the
79 solid electrolyte ionic conductivity.

80 An understanding of the practical electro-
81 chemical stability of solid electrolytes and
82 their (electro)chemical reactivity against elec-
83 trode materials is key to identifying viable
84 electrode/electrolyte combinations to engineer
85 ASSBs. Yet, the presence of buried inter-
86 faces in fully assembled devices complicates di-
87 agnosis, requiring the implementation of spe-
88 cialized tools that can provide spatially re-
89 solved information on interfacial compounds
90 present in minute concentrations. *Ex situ* in-
91 spection of half cells allows longer data ac-
92 quisition times and larger sample volumes to
93 compensate for sensitivity limitations. Au-
94 vergnot and collaborators elegantly used X-
95 ray photoelectron and Auger spectroscopies to
96 monitor the degradation of buried interfaces
97 formed between $\text{Li}_6\text{PS}_5\text{Cl}$ and three commer-

cial cathodes LiCoO_2 , $\text{LiNi}_{1/3}\text{Co}_{1/3}\text{Mn}_{1/3}\text{O}_2$, and LiMn_2O_4 .¹⁶ They isolated the oxidation products of $\text{Li}_6\text{PS}_5\text{Cl}$, namely LiCl , phosphate species, lithium polysulfides and elemental sulfur. In the same vein, Walther et al.¹⁷ demonstrated that time-of-flight secondary-ion mass spectrometry and XPS provide valuable insights into interphase compositions and their microstructures in ASSBs, including the local structure and morphology of the reaction layer between the cathode ($\text{LiNi}_{0.6}\text{Co}_{0.2}\text{Mn}_{0.2}\text{O}_2$) and the solid electrolyte ($\text{Li}_6\text{PS}_5\text{Cl}$). Remarkably, Hakari et al.¹⁸ have circumvented sensitivity issues by preparing “magnified interfaces” consisting of a composite electrode of Li_3PS_4 glass electrolyte and carbon. This composite increased the contact area with the Li metal electrode and facilitated the *ex situ* observation of electrochemical reactions and decomposition. Interfacial reactions have also been studied as a function of temperature using surface-sensitive synchrotron X-ray absorption spectroscopy and a thin film composite cathode consisting of LLZO and $\text{LiNi}_{0.6}\text{Co}_{0.2}\text{Mn}_{0.2}\text{O}_2$ to elucidate the interfacial reactions that occur during co-sintering in typical electrode fabrication processes.¹⁹ Using a related model system and time-of-flight secondary ion mass spectroscopy, Park et al.²⁰ observed compositional changes at the LLZO/ LiCoO_2 interface resulting from cross-exchange of La and Co at the interface, which could be mitigated with a Li_3BO_3 surface coating.

When it comes to *in situ* and *operando* investigations, sensitivity limitations are aggravated by the constraints imposed by full device analysis, yet several studies have provided new and important insights into key degradation processes. For example, Sang et al. examined the reactions of LGPS and Li_3PS_4 with Li metal using *in situ* and *operando* Raman and identified the reversible reduction of P(V)S_4^{3-} moieties into $\text{P(IV)}_2\text{S}_6^{4-}$.²¹ The inherent challenges in probing interfaces through experimental methods have stimulated significant efforts in the modeling area.²² Relying on the power of DFT and AIMD simulations, a robust thermodynamic framework, and database science, Tang et al.²² have developed a multi-tier approach

to investigate the chemical, electrochemical and kinetic evolution of interfaces in ASSBs. For instance, pair distribution functions derived from AIMD simulations fingerprinted on a library of simple binary compounds showed that the decomposition of the $\text{NaCoO}_2/\text{Na}_3\text{PS}_4$ interface gives rise to the formation of sulphate groups and Na_3P compounds.

Understanding and mitigating the formation of Li dendrites during cycling is an important step towards the deployment of high energy density ASSBs based on a Li metal anode. Despite the high bulk modulus of ceramic electrolytes, Li dendrites have been found to form within grain boundaries, resulting in cell shorts upon extended cycling. Using ^7Li chemical shift imaging and electron microscopy, Marbella et al.²³ monitored Li microstructural growth during galvanostatic cycling of $\text{Li}_{6.5}\text{La}_3\text{Zr}_{1.5}\text{Ta}_{0.5}\text{O}_{12}$ and correlated their findings with alterations in the voltage profiles. This study showed that magnetic resonance imaging enables to detect Li microstructures well before short-circuits. Additionally, transformations of both the stripping and plating interfaces were observed, indicating heterogeneities in both Li removal and deposition. While smooth Li electroplating has been the focus of strategies to mitigate Li dendrites, recently, a DFT and kinetic Monte Carlo study by Yang and coworkers showed that the Li stripping process is equally critical to the formation of the Li microstructure.²⁴ The authors showed that the nature of the solid electrolyte interphases at the surface of the Li metal anode played an important role in the formation of nonuniform local current densities and dendrite nucleation, suggesting that electrode coating strategies can be effective for maintaining a smooth Li surface during the stripping process.

In closing, step advances in the field rely on the identification and synthesis of new and improved ion-conductors. One traditional approach is through elemental substitution to determine the solid solution range and the impact on ionic conductivity. For instance, NaSiCONs (Sodium Super Ionic CONductor) with general formula $\text{Na}_{1+x}\text{Zr}_2\text{Si}_x\text{P}_{3-x}\text{O}_{12}$ ($0 \leq x \leq 3$) form the basis of many Na-ion solid elec-

1 trolites (but also Li-ion).²⁵ Ma et al.²⁶ and
2 later Deng et al.²⁷ have explored the partial
3 substitution of zirconium by scandium over a
4 large range of composition in the NaSiCON
5 $\text{Na}_{3+x}\text{Sc}_x\text{Zr}_{2-x}\text{Si}_2\text{PO}_{12}$ structure using a scalable
6 solution-assisted solid-state reaction method.
7 In this case, solid solutions were obtained for all
8 compositions and the highest room temperature
9 conductivity of 4.0×10^{-3} S/cm was achieved for
10 the $x = 0.4$ sample.²⁶

11 High-throughput experimental and theoretical
12 screening approaches have been used to ac-
13 celerate the identification of promising conduc-
14 tors and their synthesizabilities. A combina-
15 torial approach was recently employed to ex-
16 plore the Li-La-Ti-O pseudo-ternary phase
17 diagram,²⁸ with over 576 samples synthesized
18 and characterized by XRD. While perovskite
19 LLTOs can be obtained over a wide compo-
20 sitional range, they are never phase-pure but
21 coexist with secondary phases such as TiO_2 .
22 Recently, a guided search for fast ion conduc-
23 tors was carried out using a machine learning-
24 based prediction model for materials selec-
25 tion.²⁹ DFT-MD simulations were then used to
26 calculate ionic conductivity. Over 12,000 mate-
27 rials were screened and several new solid mate-
28 rials with predicted superionic lithium conduc-
29 tion were identified. Notably, $\text{Li}_5\text{B}_7\text{S}_{13}$ has a
30 predicted room temperature Li-ion conductiv-
31 ity of ~ 74 mS/cm, several times higher than
32 the best-known ion conductors to date.

33 While the intragrain conductivity is largely
34 determined by the crystal structure, sample
35 density and microstructure strongly influence
36 the macroscopic conductivity and must be con-
37 trolled during synthesis. *Operando* synchrotron
38 XRD and mesoscale modeling were recently
39 used to understand the effects of calcination
40 and densification on LLZO.³⁰ This study found
41 that the most effective densification is obtained
42 when small and bimodal distributions of par-
43 ticles are used. Grain boundary contributions
44 to ionic transport in LLZO were computationally
45 examined by Yu et al.³¹ Specifically, the
46 energetics, composition, and transport proper-
47 ties of several low energy symmetric tilt grain
48 boundaries in LLZO were characterized at the
49 atomic scale. While lithium transport is gener-

ally reduced in grain boundaries, the magnitude
of this effect depends on temperature and grain
boundary structure, in keeping with experimen-
tal findings.

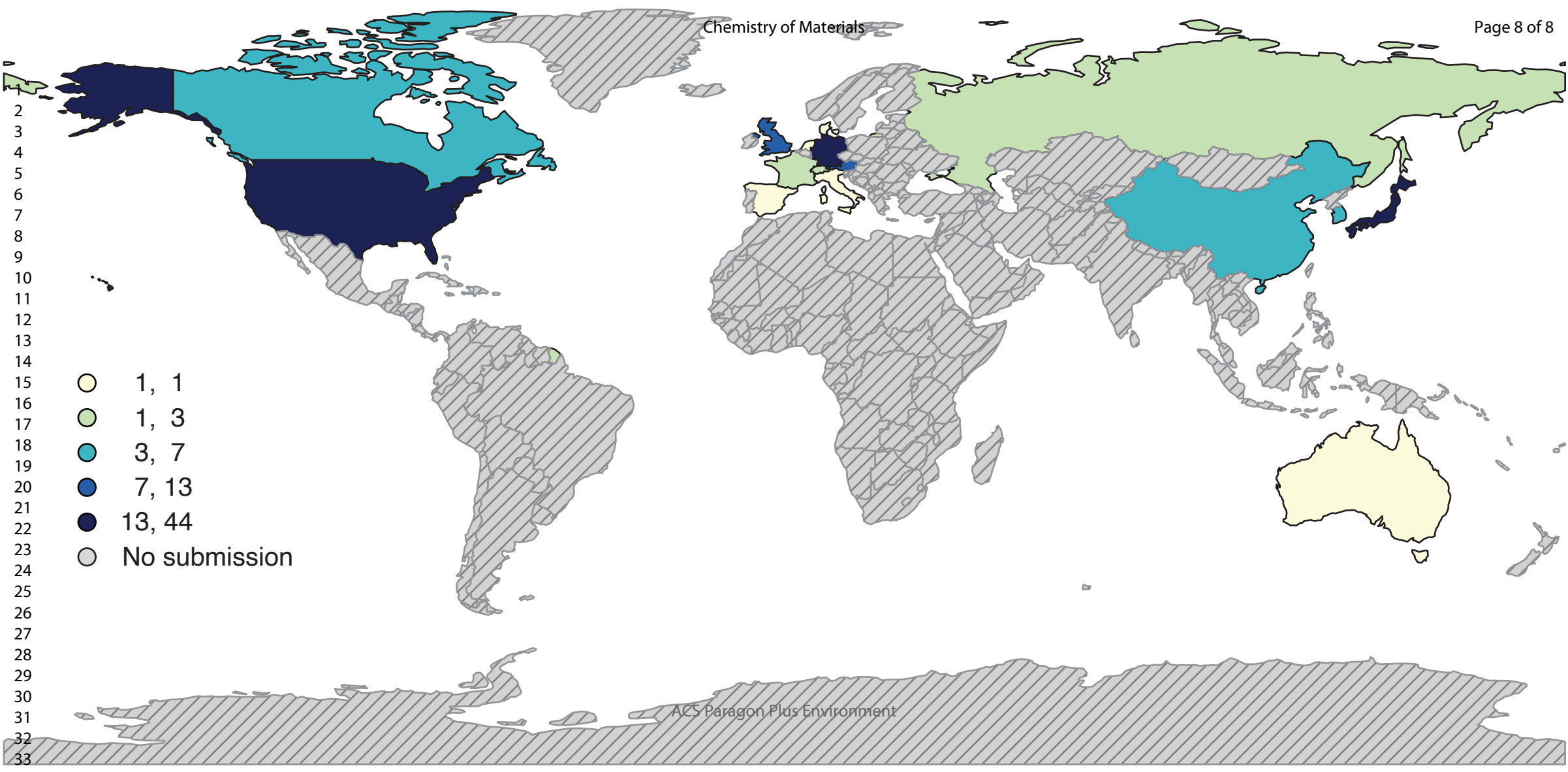
Research in solid electrolytes and their batter-
ies is exciting, fastpaced, and multidisciplinary.
New synthesis strategies, specialized *in situ* and
operando characterization measurements, and
computational techniques to probe unique phe-
nomena of ASSBs are being developed. The de-
velopment of working ASSBs certainly requires
new insights, which may be achieved through
knowledge transfer from other areas of material
science, such as, solid oxide fuel cells, semicon-
ductor technologies, functional polymers, met-
allurgy, and others.

References

- (1) de Klerk, N. J. J.; Rosłoń, I.; Wage-
maker, M. Diffusion Mechanism of Li Ar-
gyrodite Solid Electrolytes for Li-Ion Bat-
teries and Prediction of Optimized Halo-
gen Doping: The Effect of Li Vacancies,
Halogens, and Halogen Disorder. *Chem.*
Mater. **2016**, *28*, 7955–7963.
- (2) Weber, D. A.; Senyshyn, A.;
Weldert, K. S.; Wenzel, S.; Zhang, W.;
Kaiser, R.; Berendts, S.; Janek, J.;
Zeier, W. G. Structural Insights and 3D
Diffusion Pathways within the Lithium
Superionic Conductor $\text{Li}_{10}\text{GeP}_2\text{S}_{12}$.
Chem. Mater. **2016**, *28*, 5905–5915.
- (3) Suzuki, N.; Richards, W. D.; Wang, Y.;
Miara, L. J.; Kim, J. C.; Jung, I.-S.;
Tsujimura, T.; Ceder, G. Synthesis and
Electrochemical Properties of $I\bar{4}$ -Type
 $\text{Li}_{1+2x}\text{Zn}_{1-x}\text{PS}_4$ Solid Electrolyte. *Chem.*
Mater. **2018**, *30*, 2236–2244.
- (4) Famprikis, T.; Bouyanfif, H.; Canepa, P.;
Zbiri, M.; Dawson, J. A.; Suard, E.;
Fauth, F.; Playford, H. Y.; Dambour-
net, D.; Borkiewicz, O. J.; Courty, M.;
Clemens, O.; Chotard, J.-N.; Islam, M. S.;
Masquelier, C. Insights into the Rich
Polymorphism of the Na^+ Ion Con-
ductor Na_3PS_4 from the Perspective

- of Variable-Temperature Diffraction and Spectroscopy. *Chem. Mater.* **2021**, *33*, 5652–5667.
- (5) Ramos, E. P.; Zhang, Z.; Assoud, A.; Kaup, K.; Lalère, F.; Nazar, L. F. Correlating Ion Mobility and Single Crystal Structure in Sodium-Ion Chalcogenide-Based Solid State Fast Ion Conductors: $\text{Na}_{11}\text{Sn}_2\text{PnS}_{12}$ (Pn = Sb, P). *Chem. Mater.* **2018**, *30*, 7413–7417.
- (6) Hanghofer, I.; Redhammer, G. J.; Rohde, S.; Hanzu, I.; Senyshyn, A.; Wilkening, H. M. R.; Rettenwander, D. Untangling the Structure and Dynamics of Lithium-Rich Anti-Perovskites Envisaged as Solid Electrolytes for Batteries. *Chem. Mater.* **2018**, *30*, 8134–8144.
- (7) Wang, F.; Evans, H. A.; Kim, K.; Yin, L.; Li, Y.; Tsai, P.-C.; Liu, J.; Lapidus, S. H.; Brown, C. M.; Siegel, D. J.; Chiang, Y.-M. Dynamics of Hydroxyl Anions Promotes Lithium Ion Conduction in Antiperovskite Li_2OHCl . *Chem. Mater.* **2020**, *32*, 8481–8491.
- (8) Kim, K.; Park, D.; Jung, H.-G.; Chung, K. Y.; Shim, J. H.; Wood, B. C.; Yu, S. Material Design Strategy for Halide Solid Electrolytes Li_3MX_6 (X = Cl, Br, and I) for All-Solid-State High-Voltage Li-Ion Batteries. *Chem. Mater.* **2021**, *33*, 3669–3677.
- (9) Helm, B.; Schlem, R.; Wankmiller, B.; Banik, A.; Gautam, A.; Ruhl, J.; Li, C.; Hansen, M. R.; Zeier, W. G. Exploring Aliovalent Substitutions in the Lithium Halide Superionic Conductor $\text{Li}_{3-x}\text{In}_{1-x}\text{Zr}_x\text{Cl}_6$ ($0 \leq x \leq 0.5$). *Chem. Mater.* **2021**, *33*, 4773–4782.
- (10) Harm, S.; Hatz, A.-K.; Moudrakovski, I.; Eger, R.; Kuhn, A.; Hoch, C.; Lotsch, B. V. Lesson Learned from NMR: Characterization and Ionic Conductivity of LGPS-like Li_7SiPS_8 . *Chem. Mater.* **2019**, *31*, 1280–1288.
- (11) Marple, M. A.; Aitken, B. G.; Kim, S.; Sen, S. Fast Li-Ion Dynamics in Stoichiometric $\text{Li}_2\text{S}-\text{Ga}_2\text{Se}_3-\text{GeS}_2$ Glasses. *Chem. Mater.* **2017**, *29*, 8704–8710.
- (12) Krasnikova, I. V.; Pogosova, M. A.; Sanin, A. O.; Stevenson, K. J. Toward Standardization of Electrochemical Impedance Spectroscopy Studies of Li-Ion Conductive Ceramics. *Chem. Mater.* **2020**, *32*, 2232–2241.
- (13) Li, W.; Liang, J.; Li, M.; Adair, K. R.; Li, X.; Hu, Y.; Xiao, Q.; Feng, R.; Li, R.; Zhang, L.; Lu, S.; Huang, H.; Zhao, S.; Sham, T.-K.; Sun, X. Unraveling the Origin of Moisture Stability of Halide Solid-State Electrolytes by *In Situ* and *Operando* Synchrotron X-Ray Analytical Techniques. *Chem. Mater.* **2020**, *32*, 7019–7027.
- (14) Sharafi, A.; Kazyak, E.; Davis, A. L.; Yu, S.; Thompson, T.; Siegel, D. J.; Dasgupta, N. P.; Sakamoto, J. Surface Chemistry Mechanism of Ultra-Low Interfacial Resistance in the Solid-State Electrolyte $\text{Li}_7\text{La}_3\text{Zr}_2\text{O}_{12}$. *Chem. Mater.* **2017**, *29*, 7961–7968.
- (15) Brugge, R. H.; Hekselman, A. K. O.; Cavallaro, A.; Pesci, F. M.; Chater, R. J.; Kilner, J. A.; Aguadero, A. Garnet Electrolytes for Solid State Batteries: Visualization of Moisture-Induced Chemical Degradation and Revealing Its Impact on the Li-Ion Dynamics. *Chem. Mater.* **2018**, *30*, 3704–3713.
- (16) Auvergniot, J.; Cassel, A.; Ledeuil, J.-B.; Viallet, V.; Seznec, V.; Dedryvère, R. Interface Stability of Argyrodite $\text{Li}_6\text{PS}_5\text{Cl}$ toward LiCoO_2 , $\text{LiNi}_{1/3}\text{Co}_{1/3}\text{Mn}_{1/3}\text{O}_2$, and LiMn_2O_4 in Bulk All-Solid-State Batteries. *Chem. Mater.* **2017**, *29*, 3883–3890.
- (17) Walther, F.; Koerver, R.; Fuchs, T.; Ohno, S.; Sann, J.; Rohnke, M.; Zeier, W. G.; Janek, J. Visualization of the Interfacial Decomposition of Composite Cathodes in Argyrodite-Based

- All-Solid-State Batteries Using Time-of-Flight Secondary-Ion Mass Spectrometry. *Chem. Mater.* **2019**, *31*, 3745–3755.
- (18) Hakari, T.; Deguchi, M.; Mitsuhashi, K.; Ohta, T.; Saito, K.; Orikasa, Y.; Uchiyama, Y.; Kowada, Y.; Hayashi, A.; Tatsumisago, M. Structural and Electronic-State Changes of a Sulfide Solid Electrolyte during the Li Deinsertion–Insertion Processes. *Chem. Mater.* **2017**, *29*, 4768–4774.
- (19) Kim, Y.; Kim, D.; Bliem, R.; Vardar, G.; Waluyo, I.; Hunt, A.; Wright, J. T.; Katsoudas, J. P.; Yildiz, B. Thermally Driven Interfacial Degradation between $\text{Li}_7\text{La}_3\text{Zr}_2\text{O}_{12}$ Electrolyte and $\text{LiNi}_{0.6}\text{Mn}_{0.2}\text{Co}_{0.2}\text{O}_2$ Cathode. *Chem. Mater.* **2020**, *32*, 9531–9541.
- (20) Park, K.; Yu, B.-C.; Jung, J.-W.; Li, Y.; Zhou, W.; Gao, H.; Son, S.; Goodeenough, J. B. Electrochemical Nature of the Cathode Interface for a Solid-State Lithium-Ion Battery: Interface between LiCoO_2 and Garnet- $\text{Li}_7\text{La}_3\text{Zr}_2\text{O}_{12}$. *Chem. Mater.* **2016**, *28*, 8051–8059.
- (21) Sang, L.; Haasch, R. T.; Gewirth, A. A.; Nuzzo, R. G. Evolution at the Solid Electrolyte/Gold Electrode Interface during Lithium Deposition and Stripping. *Chem. Mater.* **2017**, *29*, 3029–3037.
- (22) Tang, H.; Deng, Z.; Lin, Z.; Wang, Z.; Chu, I.-H.; Chen, C.; Zhu, Z.; Zheng, C.; Ong, S. P. Probing Solid–Solid Interfacial Reactions in All-Solid-State Sodium-Ion Batteries with First-Principles Calculations. *Chem. Mater.* **2018**, *30*, 163–173.
- (23) Marbella, L. E.; Zekoll, S.; Kasemchainan, J.; Emge, S. P.; Bruce, P. G.; Grey, C. P. ^7Li NMR Chemical Shift Imaging To Detect Microstructural Growth of Lithium in All-Solid-State Batteries. *Chem. Mater.* **2019**, *31*, 2762–2769.
- (24) Yang, C.-T.; Qi, Y. Maintaining a Flat Li Surface during the Li Stripping Process via Interface Design. *Chem. Mater.* **2021**, *33*, 2814–2823.
- (25) Deng, Z.; Sai Gautam, G.; Kolli, S. K.; Chotard, J.-N.; Cheetham, A. K.; Masquelier, C.; Canepa, P. Phase Behavior in Rhombohedral NaSiCON Electrolytes and Electrodes. *Chem. Mater.* **2020**, *32*, 7908–7920.
- (26) Ma, Q.; Guin, M.; Naqash, S.; Tsai, C.-L.; Tietz, F.; Guillon, O. Scandium-Substituted $\text{Na}_3\text{Zr}_2(\text{SiO}_4)_2(\text{PO}_4)$ Prepared by a Solution-Assisted Solid-State Reaction Method as Sodium-Ion Conductors. *Chem. Mater.* **2016**, *28*, 4821–4828.
- (27) Deng, Y.; Eames, C.; Nguyen, L. H. B.; Pecher, O.; Griffith, K. J.; Courty, M.; Fleutot, B.; Chotard, J.-N.; Grey, C. P.; Islam, M. S.; Masquelier, C. Crystal Structures, Local Atomic Environments, and Ion Diffusion Mechanisms of Scandium-Substituted Sodium Superionic Conductor (NASICON) Solid Electrolytes. *Chem. Mater.* **2018**, *30*, 2618–2630.
- (28) Jonderian, A.; Ting, M.; McCalla, E. Metastability in Li–La–Ti–O Perovskite Materials and Its Impact on Ionic Conductivity. *Chem. Mater.* **2021**, *33*, 4792–4804.
- (29) Sendek, A. D.; Cubuk, E. D.; Antoniuk, E. R.; Cheon, G.; Cui, Y.; Reed, E. J. Machine Learning-Assisted Discovery of Solid Li-Ion Conducting Materials. *Chem. Mater.* **2019**, *31*, 342–352.
- (30) Barai, P.; Fister, T.; Liang, Y.; Libera, J.; Wolfman, M.; Wang, X.; Garcia, J.; Iddir, H.; Srinivasan, V. Investigating the Calcination and Sintering of $\text{Li}_7\text{La}_3\text{Zr}_2\text{O}_{12}$ (LLZO) Solid Electrolytes Using Operando Synchrotron X-Ray Characterization and Mesoscale Modeling. *Chem. Mater.* **2021**, *33*, 4337–4352.
- (31) Yu, S.; Siegel, D. J. Grain Boundary Contributions to Li-Ion Transport in the Solid Electrolyte $\text{Li}_7\text{La}_3\text{Zr}_2\text{O}_{12}$ (LLZO). *Chem. Mater.* **2017**, *29*, 9639–9647.



1
2
3
4
5
6
7
8
9
10
11
12
13
14
15
16
17
18
19
20
21
22
23
24
25
26
27
28
29
30
31
32
33